

MULTI-PHASE SYNCHRONOUS MOTOR SOLUTION FOR STEERING APPLICATIONS

A. R. Matyas, K. A. Biro, and D. Fodorean*

Electrical Machines and Drives Department, Technical University of Cluj-Napoca, 28 Memorandumului, Cluj-Napoca 400114, Romania

Abstract—This paper presents the analysis of a six-phase permanent magnet synchronous machine (PMSM6) dedicated for electrical power steering system applications. The motor design is briefly described, as well as the construction of the studied motor. The study is validated by finite element method and via experimental results. Some simulated results prove the machine's capability to work even in faulty conditions. The operation of the machine was evaluated in generator and motor operation. In motor operation, the PMSM6 was fed based on scalar control.

1. INTRODUCTION

The general trend in automotive industry, regarding the auxiliary subsystems (like the steering system, ventilation/heating, braking etc.) is to use more and more electric actuators, thus increasing comfort and safety and helping to improve performance, reduce fuel consumption and emissions. Average number of existing electric motors in a car is somewhere in the figure 30 and will grow in the future to 100 [1–4].

The most important actors in automotive industries have gathered to establish the new demands of automobiles in terms of fuel consumption, gas emission and on-board available energy. Programs like the Partnership for a New Generation of Vehicles or Consortium for Advanced Automotive Electrical/Electronic Components and Systems have established the new voltage standard level for the power net, to 42 V [5, 6]. Moreover, the electrical power needed in the future, for the steady state regime of auxiliary subsystem, is estimated to be in the range of 3000 W... 7000 W. On board of an automobile are many classical subsystems (hydraulic or mechanical ones) which

Received 5 June 2012, Accepted 31 July 2012, Scheduled 4 September 2012

* Corresponding author: Daniel Fodorean (daniel.fodorean@emd.utcluj.ro).

can be replaced by the electrical solutions, the goal being, finally, the elimination of fuel consumption (thus reducing to zero the gas emissions). One of these subsystems is the steering system.

The first electrically assisted steering systems (electrical power steering — EPS), appeared in the late 80s, by which an electric motor was used to produce torque assistance, thus replacing the hydraulic system. Key parameters in choosing electric motors for power steering systems are high torque density, low torque ripples, low noise and energy efficiency.

When designing an EPS drive system, several requirements have to be considered: its reliability, output performance, thermal and acoustic behavior, high energy efficiency and reduced costs. In order to fulfill these requirements, the application demands high performance motors with high power density and high dynamics, reduced torque ripples and low radial forces [2].

Moreover, the EPS system should be able to continue its operation even in the event of the failure of (one or more faults within) some of its components (drive, electrical machine or sensors). The capability to operate even if a fault occurred is called fault tolerance. When trying to construct an EPS which is fault tolerant, the designing process can be focused either on the power electronic converter, or on the electrical machine structure. The use of poly-phase machines and drives against conventional three-phase machines results in a more fault tolerant system, because when a fault occurs on one or several phases, the machine will still be capable to operate, with acceptable output mechanical performances which are limited only by the windings thermal harshness [7–11]. This is the major advantage of the multi-phase drive-machine system. On the other hand, a problem appears when trying to control such a complex subsystem.

When using a high number of phases, the controllability of the system is more difficult to be employed. In embedded systems, when more than 4 phases are in use, the common microcontrollers found on the market cannot meet the controllability requirements (usually, a microcontroller has 3/6 or 4/8 PWM generators). Thus, for a system with 6 phases are needed at least two microcontrollers. The synchronization of the microcontrollers is very difficult to be employed. In order to solve the problem, the authors are proposing a special winding configuration which will assure the motor supplying only via one microcontroller device, based on 3/6 PWM generators. The use of a six-phase machine with symmetrical 60 degrees displacement windings allows a high reliability.

For a specific EPS main data design, the major achievements of this research work are the proposition of a fault tolerant 6 phase PMSM

machine with its power drive and control unit, based on simplified control technique. The study is employed analytically, numerically (through finite element method — FEM) and through tests.

2. MAIN DATA DESIGN

For the EPS application, based on a literature review, we have found several variants of electrical machines solutions [1, 2, 5, 6]. From induction motor to synchronous and switched reluctance motor, the researchers have tried to explain and exploit the advantages of each proposition. Since in terms of power density and efficiency the synchronous motor, excited with permanent magnets, represents the best variant, the authors have made their choice: the permanent magnet synchronous machine (PMSM). One of the weak points of the PMSM is the pulsating torque characteristic. To overcome this drawback, one of the solutions will be the use of more than three stator phases. There is another possibility to decrease the torque ripple: by skewing the stator of the machine, or through proper control (by controlling the direct and quadrature axis currents). But both solutions will decrease the average torque [6]. So a supplementary current will be needed to reach the desired torque (the increase of current will increase, finally, the copper loss, while the efficiency decreases). Thus, we will take advantage of a six phase machine (PMSM6), while the controllability needs to be carefully employed. Several advantages can be noted when using multi-phase machine-drive: lower current per phase for a given voltage rating, lower amplitude of torque pulsations, lower copper loss for the harmonics when a voltage source inverter (VSI) is used and the ability of the motor to start and run with one or more open phases [6].

The output performances of steering system, used on board of automobile, demand: high reliability, reduced investment, size and mass, low noise level and capability to operate in a wide speed range (in the constant power region of the torque-speed characteristic). All these criteria should be considered in the design process of the EPS.

EPS solutions can be separated into categories by the location of the electric motor that provides steering assistance, as: column, pinion, rack, and double pinion. Most of the EPS systems proposed by industry for small and middle size vehicles are mounted on the pinion steering gear, or on the steering column, eliminating parasitic losses normally associated with hydraulic power steering systems.

Both configurations require, as key performance parameters, high torque density, very low cogging torque, low acoustic noise and high efficiency.

Analyzing the different electrical actuators currently in use, the maximum torque/speed characteristic associated to the steering column correspond to an operating point chosen to a maximum assisted torque of 15 Nm at a steering wheel speed of 120 rpm. The actuator is coupled to the steering shaft via a transmission with a gear ratio usual for this type of application.

A high rotational speed ensures a low volume and an easier winding for the six-phase machine. The maximum operating speed will be set at 3000 rpm which can be obtained with a 2 poles machine driven at 50 Hz. In practice, the maximum speed of rotation of the steering wheel is 2 rotations per second which corresponds to 120 rpm. So, to achieve the maximum operation speed, we need a gear ratio of 1/25. For a fixed rated torque of 0.3 Nm, which is multiplied by the gear ratio, corresponds to an assistance torque of 7.5 Nm. The last can provide an adequate assistance for the small vehicles and it is easy to achieve twice the rated torque at startup without heat and saturation constraint.

2.1. The Stator of the Proposed PMSM6

The design of the PMSM6 can start by the expression of the air-gap diameter or by the expression of the magnet volume needed to produce the desired power [8, 12–18]. High performance optimization algorithms (genetic or evolutionary type) can be included into the design process [19–22], in order to improve the power density of the studied machine. The analytical approach used for the designed machine is not presented here, the author willing to emphasize clearly the numerical and experimental results. Several details of the analytical model will be given when evaluating the armature reaction effect. Thus, here only the main geometrical parameters will be presented. The stator sheet of the proposed PMSM6 has 24 slots, as it can be seen in Figure 1.

In Table 1 are presented the main parameters of the PMSM6. The main task for designing the PMSM6 is the layout of the six-phase stator winding and the topology of the rotor.

2.2. The Winding of the Studied PMSM6

Usually, the machine's number of phases is assumed to be the same as the number of stator terminals (excluding the neutral). However, giving number of phases is not always an adequate description. This is the case because for a given number of phases on a machine, two variants are possible based on the possible values of the phase belt angle. Almost all three-phase motors have 60° phase belts or,

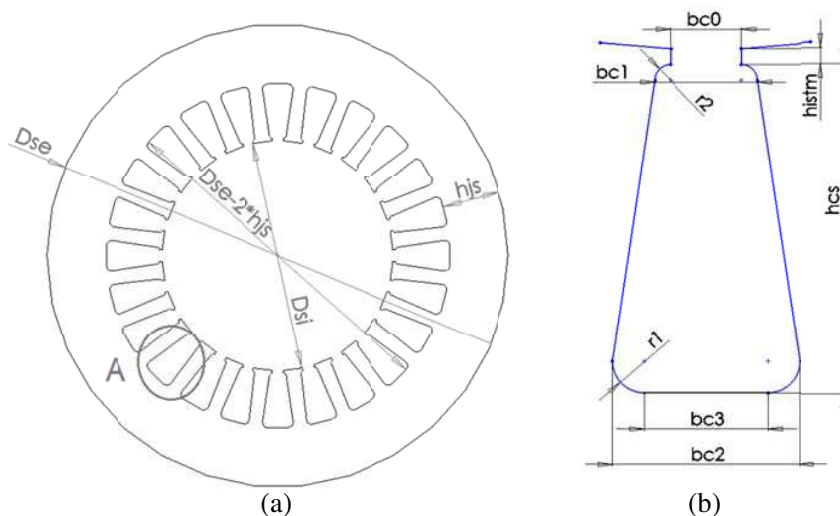


Figure 1. (a) Dimensions of the stator sheet. (b) Slot's details.

Table 1. Stator and rotor dimensions of PMSM6.

Number of stator slots	24
Stator outer diameter (Dse)	90 mm
Stator inner diameter (Dsi)	45 mm
Stator yoke height (hjs)	11.5 mm
Stack length	40 mm
Rotor outer diameter	44.2 mm
Stator slot opening (bc0)	2.25 mm
Stator slot height (hcs)	10.5 mm
Minimum width of stator slot (bc1)	3.25 mm
Maximum width of stator slot (bc2)	5.92 mm

occasionally, 120° phase belts and they have some characteristics which are different from the 60° variants.

It is convenient to specify the number of phase belts per pole when designing the winding of a machine. The parameter q' will be used for the expression of the phase belt per pole, being obtained with the following equation:

$$q' = \frac{180}{\beta} \tag{1}$$

where β is the phase belt in electrical degrees.

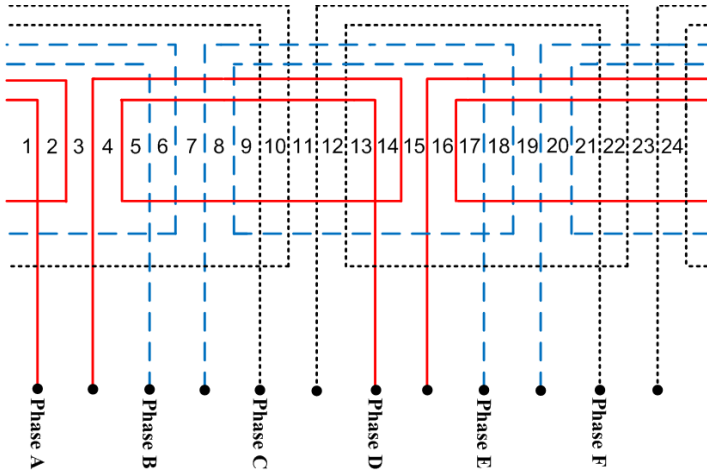


Figure 2. PMSM6 stator windings.

For a six-phase machine the phase belt angle β is 60° , the number of phase belts per pole q' is 3. In Figure 2 is presented the layout for a star-connected six-phase machine with distributed winding configuration. In this stator winding, each phase is made of a single coil.

The six phases are spaced shifted by 60° and the phase-shift is 60° between phase axes. For the 24 stator slots, 12 coils are used to complete the winding. The phase A winding starts in slot 1 and continues in slots 17, 2 and 16 (see Figure 2). For the phases B, C, D, E and F, they are placed in different slots by moving $4/3$ of a pole (4 slots pitches). All coils/phase are connected in series to form one current path. Starting from these parameters, the total flux, the number of conductors per slot as well as the cross section of the wire can be computed using simple analytical formula (not presented here).

2.3. The Rotor of the Proposed PMSM6

For the design of the rotor topology of the PMSM6, the goal is to decrease the size of the PMs and, finally, of the cost of the machine. Different types of rotors exist (with PMs placed on the surface, inset to realize to flux-concentrated variant or berried on one or several layers) and they all will influence the aforementioned goal. A criteria of choosing the rotor structure can be the application itself (if it is intending to work in a wide speed rage, the surface mounted variant, which gives the best power density, will not be the first choice; inset or

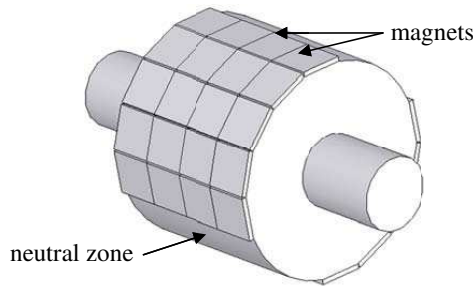


Figure 3. PMSM6 rotor with the magnets placed on the rotor.

berried magnets variant should be used). Also, another criteria could be the manufacturing difficulties. If the PMs have high remanent flux density, it is difficult to inset the PMs within the rotor iron. In our case, we want to have the best power density, thus the surface mounted topology should be used. The design of the rotor structure has not to be complex; an easiness of the manufacturing process must be kept in mind for a future industrial application. Other objectives are the torque ripple and dynamic behavior of the machine, which will be examined also in the next sections.

After the total magnet volume was calculated, the dimension of the magnetic pole piece was obtained. Due to the 1 mm height and the arc shape form, the magnet couldn't be produced on one piece. Thus, another solution was found: to use existing block shape magnets that can be found on the market: many PMs pieces mounted on the surface of the rotor, oriented in the same magnetic direction, to form a magnetic pole, see Figure 3.

2.4. The Magnetic Equivalent Circuit

The nonlinearity of the magnetic core has been taken into account. For that, the magnetic equivalent circuit of the PMSM6 was drawn, Figure 4. The advantage of the proposed lumped equivalent circuit is due to the fact that it takes into consideration the armature reaction effect. The flux density level in each active part of the machine is calculated based on the steel magnetic characteristic.

A magnetic equivalent circuit has one or more closed loop paths, and contains one or more magnetic fluxes. Usually, the flux is generated by a magnetic field source — permanent magnets or electromagnets — and confined to the path by magnetic cores. In the study of the armature reaction the magnetic field sources are the PMs.

To determine the flux densities in the PMSM6, the coil's

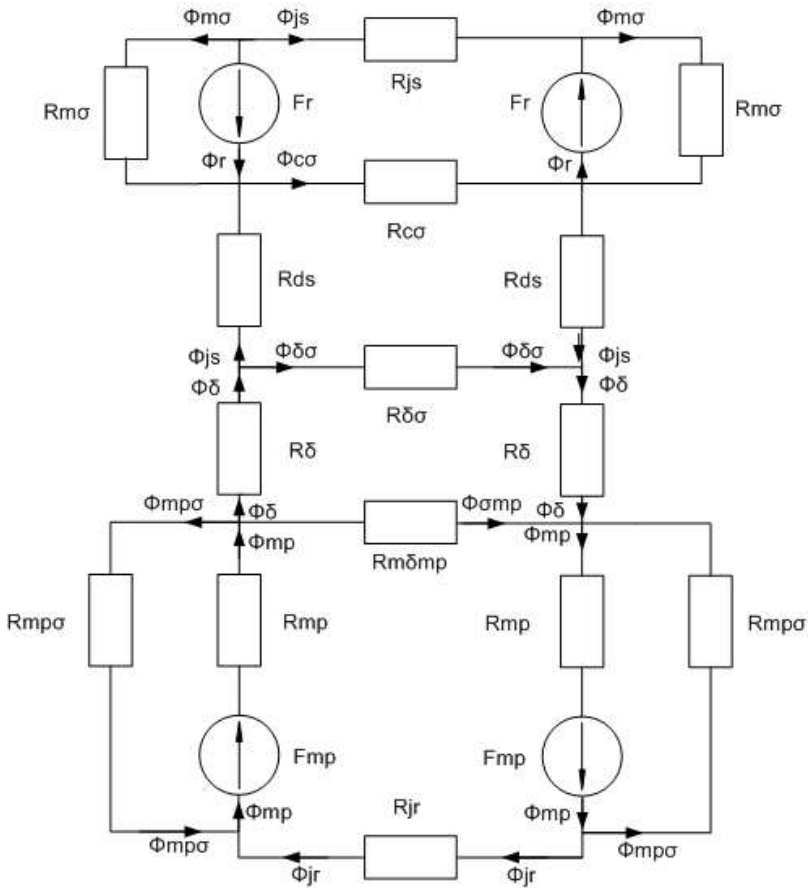


Figure 4. The PMSM6 magnetic equivalent circuit, with armature reaction.

magnetomotive force is introduced. The Equations (2) to (12) represent the analytical expression of the magnetic behavior of the studied machine.

$$2 \cdot F_{mp} + 2 \cdot R_{mp} \cdot \Phi_{mp} + \Phi_{\sigma mp} \cdot R_{m\sigma mp} + \Phi_{jr} \cdot R_{jr} = 0 \quad (2)$$

$$\Phi_{mp} \cdot R_{mp} + \Phi_{mp\sigma} \cdot R_{mp\sigma} + F_{mp} = 0 \quad (3)$$

$$-\Phi_{c\sigma} \cdot R_{c\sigma} + \Phi_{js} \cdot R_{js} - 2 \cdot F_r = 0 \quad (4)$$

$$\Phi_{m\sigma} \cdot R_{m\sigma} + F_r = 0 \quad (5)$$

$$2 \cdot \Phi_{\delta} \cdot R_{\delta} + \Phi_{\delta\sigma} \cdot R'_{\delta\sigma} - \Phi_{\sigma mp} \cdot R_{m\sigma mp} = 0 \quad (6)$$

$$2 \cdot \Phi_{ds} \cdot R_{ds} + \Phi_{c\sigma} \cdot R_{c\sigma} - \Phi_{\delta\sigma} \cdot R'_{\delta\sigma} = 0 \quad (7)$$

$$\Phi ds - \Phi c\sigma - \Phi r + \Phi m\sigma = 0 \tag{8}$$

$$\Phi r - \Phi m\sigma - \Phi ds = 0 \tag{9}$$

$$\Phi jr + \Phi mp\sigma - \Phi mp = 0 \tag{10}$$

$$\Phi mp - \Phi \delta - \Phi mp\sigma - \Phi \sigma mp = 0 \tag{11}$$

$$\Phi \delta - \Phi \delta\sigma - \Phi ds = 0 \tag{12}$$

The following notation was used: $Rmp\sigma$ — the leakage reluctance of PM; Rmp — the magnetic reluctance of the PM; $R\delta$ — the reluctance of the air-gap; $R\delta\sigma$ — the leakage reluctance of the air-gap; Rds — the magnetic reluctance in the stator tooth; Rjs — the magnetic reluctance in the stator yoke; Rjr — the magnetic reluctance in the rotor yoke; $Rm\sigma mp$ — leakage reluctance between consecutive PMs; $Rc\sigma$ — the leakage reluctance of the stator slot; $Rm\sigma$ — the frontal leakage reluctance of the winding; $Rd\sigma$ — the leakage reluctance of the stator tooth to the air-gap; Fmp — magnetomotive-force of the PM; Fr — the magnetomotive-force of the armature reaction. The Φ parameter refers to the magnetic flux, while the associated indices (i.e., mp , σ , δ , ds etc.) refer to the circuit elements indicated by the specific magnetic reluctances.

The flux density values obtained after the calculation are presented in Table 2, where Byr is the rotor yoke flux density, Bys is the stator yoke flux density, Bt is the stator teeth flux density and $B\delta 1$ is the air-gap flux density.

For an electrical machine, the magnetic flux or the flux density is the key element in the design process. Starting from these ones, it is possible to evaluate the electromagnetic parameters of the machine (i.e., the magnetic reactances in the direct and quadrature axis and the phase resistance; having those parameters we can obtain the impedance in the direct and quadrature axis, Zd and Zq respectively).

Next, the main characteristics are presented. We will start with the calculation of the induced electromotive force (in rms value), knowing that the ratio between the line and phase voltages, $r1f$, is

Table 2. Flux density values of the PMSM6.

Parameter	Unity	With armature reaction	Without armature reaction
Byr	T	0.83	0.982
Bys	T	1.192	1.448
Bt	T	1.117	1.349
$B\delta 1$	T	0.537	0.636

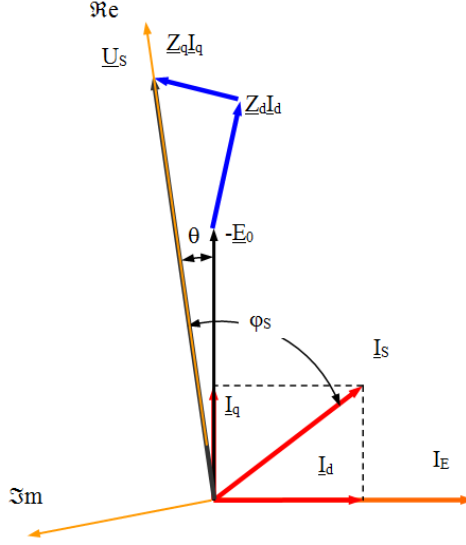


Figure 5. PMSM6's phasor diagram.

equal to unity for our 6 phase machine:

$$E = \sqrt{2} \cdot \pi \cdot p \cdot ws \cdot \Phi \delta \cdot r1f \cdot ns \quad (13)$$

where p represents the number of pole pairs, ws is the number of turns per phase and ns is the synchronous speed.

Based on the phasor-diagram of the PMSM6, Figure 5, one can get the direct and quadrature axis currents (I_d and I_q , respectively):

$$I_s = \sqrt{I_d^2 + I_q^2} \quad (14)$$

$$I_d = \frac{U_s \cdot \sin(\alpha q - \theta) - E \cdot \sin(\alpha q)}{Z_d \cdot \cos(\alpha d - \alpha q)} \quad (15)$$

$$I_q = \frac{U_s \cdot \cos(\alpha d - \theta) - E \cdot \cos(\alpha d)}{Z_q \cdot \cos(\alpha d - \alpha q)} \quad (16)$$

where αd is the angle for the direct axis impedance Z_d , αq is the angle of the quadrature axis impedance, Z_q , U_s is the source voltage.

The input power is get from the following expression:

$$P_{in} = nph \cdot \frac{U_s^2}{\cos(\alpha d - \alpha q)} \cdot \left[\frac{\cos(\alpha d - \theta) \cdot \cos(\theta)}{Z_q} - \frac{\sin(\alpha q - \theta) \cdot \sin(\theta)}{Z_d} \right] - nph \cdot \frac{U_s^2}{\cos(\alpha d - \alpha q)} \cdot \left[\frac{\cos(\alpha d) \cdot \cos(\theta)}{Z_q} - \frac{\sin(\alpha q) \cdot \sin(\theta)}{Z_d} \right] \quad (17)$$

where nph is the number of phases.

From the input power, we can get the output one, based on the classical expression:

$$P_{out} = P_{in} - \sum \text{Losses} \quad (18)$$

(The, “sum of losses” term contains the copper, iron and mechanical losses.)

Finally, the torque of the PMSM6 is:

$$T = \frac{P_{out}}{2 \cdot \pi \cdot \frac{ns}{60}} \quad (19)$$

The energetic performances (i.e., efficiency and power factor) of the designed PMSM6 are:

$$\eta = \frac{P_{out}}{P_{in}} \quad (20)$$

$$\cos \varphi = \frac{P_{in}}{nph \cdot U_s \cdot I_s} \quad (21)$$

The employed analytical approach has been given expected values, in terms of magnetic results, thus, we need to verify numerically the motor’s capability to operate in correspondence with our application. This numerical analysis is employed through a finite element method (FEM).

3. NUMERICAL ANALYSIS OF THE PROPOSED PMSM6

The finite element method software JMAG Studio was used to simulate the six-phase permanent magnets synchronous machine. The numerical analysis based on finite element method was employed on a 2D model. The transient response analysis module was used to simulate the machine’s magnetic behavior. As a result, the electromagnetic torque, the magnetic field density and the induced electromotive force along the air-gap are computed. The simulations were made in no-load and load regime and the results are presented in Figures 6–11. For the measurements in load operation, the results were obtained at rated current value.

For the induced electromotive force (Figure 6), a Fast Fourier Transformation (FFT) was applied and the space harmonics content of the induced electromotive force was computed see Figure 7.

The 3rd harmonic and the 23rd have higher values; these appear because of the PMSM6 construction. The 3rd harmonic represents 10.86% of the fundamental value.

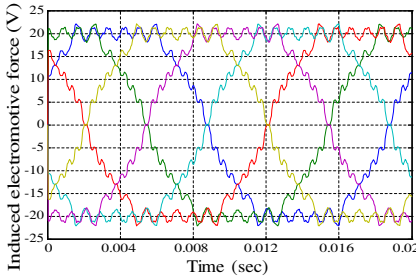


Figure 6. No-load induced electromotive force of PMSM6.

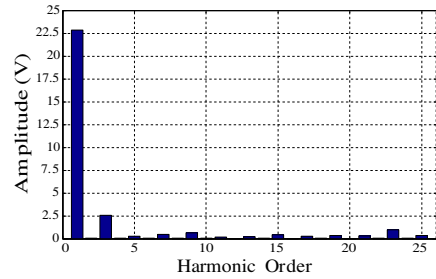


Figure 7. Harmonic content of the induced phase voltage.

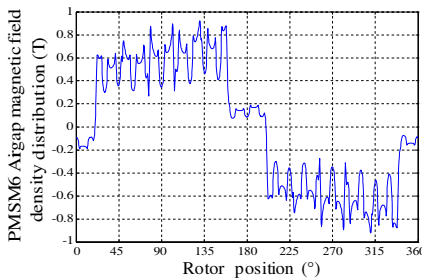


Figure 8. Magnetic field density distribution along the air-gap.

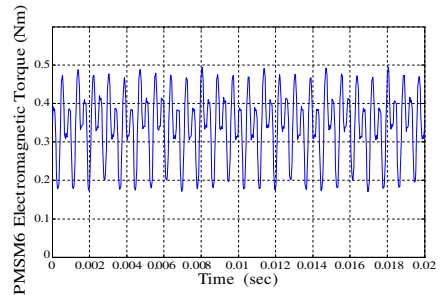


Figure 9. Electromagnetic torque.

The magnetic field density along the air-gap in load regime is presented in Figure 8. The armature reaction can be noticed. The electromagnetic torque is represented in Figure 9, the torque ripples are influenced by the cogging torque, due to the strong permanent magnets used and the rotor magnetic poles construction. The mean value of the obtained electromagnetic torque is 0.341 Nm, which is very good for our application. On a contrary, the torque ripples are quite high for such a topology, where a high power density is requested. We can see how the torque waves vary between a maximum value of 0.49 Nm and a minimum of 0.18 Nm. We will see how this value is affected by faults and if we could still operate even in most severe faulted conditions.

Several simulations were made for the purpose of the fault-tolerant aspect of the machine. The PMSM6 was simulated with one and two consecutive open phase fault. The electromagnetic torque obtained is plotted in Figures 10 and 11.

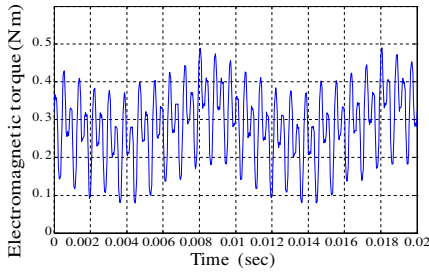


Figure 10. Electromagnetic torque — one open phase.

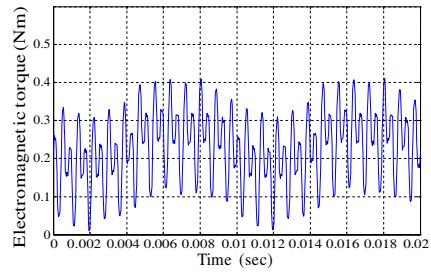


Figure 11. Electromagnetic torque — two open phases.

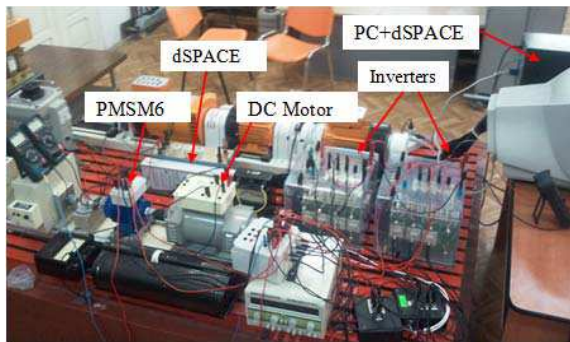


Figure 12. The PMSM6 test bench.

The mean value of the electromagnetic torque for open phase operating of the PMSM6 is 0.284 Nm, which represents 83.28% from the mean value in no fault operation. The electromagnetic torque for two open phase operating is 0.227 Nm, 66.57% from the no fault torque value. For this worst case, the torque is varying between the minimum value of 0.05 Nm value and a maximum of 0.4 Nm. But we are still satisfied by the fact that even for very severe operating conditions the machine can still operate. In order to improve the quality of the wave profile (to have a smoother torque), we should provide a specific control technique which could compensate the torque ripples (not discussed here).

Thanks to these simulated results, one could say that the analytical approach was validated since the expected results, in terms of torque development, were obtained.

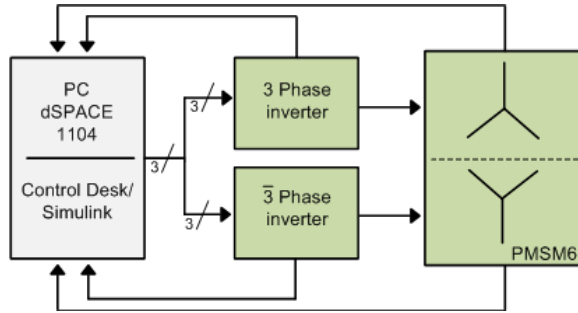


Figure 13. Block diagram of the test bench.

4. EXPERIMENTAL MEASUREMENTS AND RESULTS

To determine the characteristics of the proposed PMSM6, a test bench was built, as shown in Figure 12, while the electric diagram used for testing the machine is shown in Figure 13. The test bench consists of: the proposed PMSM6, a DC motor used as a load, 2 three phase Semikron SemiTeach inverters, PC+dSPACE for the control of the energy flow in the system, current transducers, incremental encoder of 2048 resolution for speed measuring. The control strategy was employed in dSPACE 1104. For simplicity a scalar control technique was built in Simulink. Since the hardware PWM generator available on the dSPACE board is of three phase type for the second star of the PMSM6 winding an inverse signal was used. This is the advantage of this six phase configuration, which permits the use of only 3/6 PWM generators to control 12 switches of the 2 inverters.

Different measurements were made for different load operation. The rated load conditions of the PMSM6 behaves like expected. The six phase currents are plotted in Figure 14, where the switching frequency is visible on the current waveform.

To determine the output performances of the PMSM6 constructed prototype, different levels of load were used, thus the following characteristics were obtained, see Figures 15–18. The output performances plotted in these figures represent a comparison between the values obtained analytically and the ones obtained after the experimental measurements.

The value of the stator current obtained experimentally is higher with 0.3 A at the same output power, at 81.639 W the stator current is 1.601 A. The efficiency and power factor are almost the same, so we have proved that the PMSM6 performance results obtained after analytical calculation and finite element method are correct.

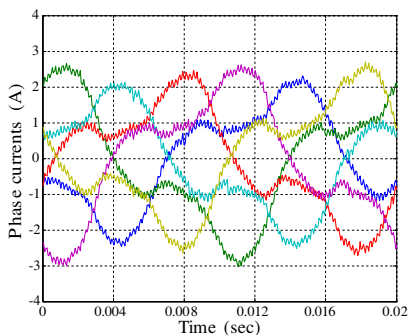


Figure 14. The PMSM6 stator currents.

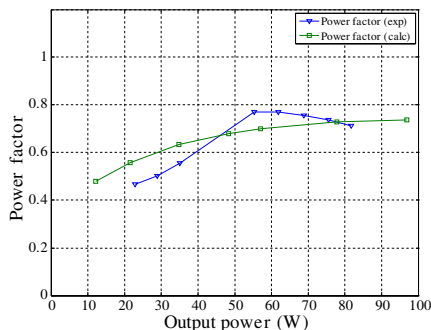


Figure 15. Comparison between measured and calculated power factor.

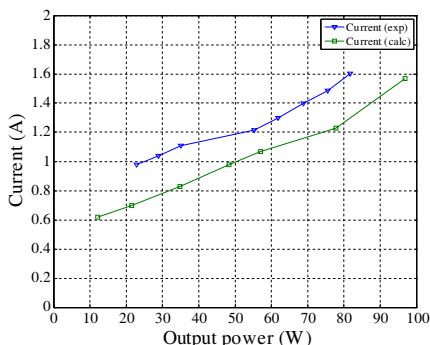


Figure 16. Comparison between measured and calculated stator current.

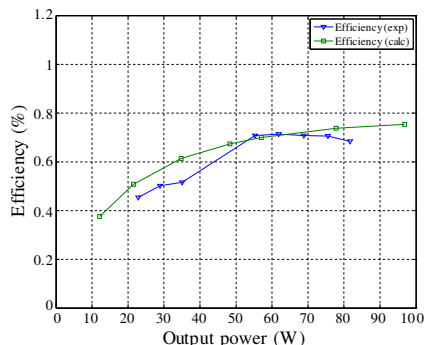


Figure 17. Comparison between measured and calculated efficiency.

Another comment is needed with respect to the comparison between the calculated and experimental results, let's say, on the current characteristic, where for the same output power of 70 W the difference is equal to 0.233 A, meaning 19%. This difference is common in electrical machine since the leakage inductance cannot be precisely calculated. The winding of the machine is made manually, thus the human error interfere here. We know from the literature that the difference between the calculated inductance leakage and the experimental obtained one is about 15–25% [8, 12].

The calculated results were obtained based on the analytical approach presented in Equations (13)–(21). Finally we can conclude that our analytical approach was validated.

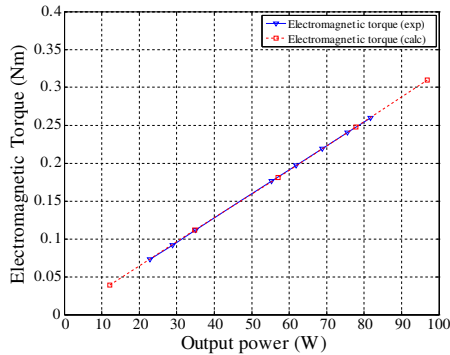


Figure 18. Comparison between measured and calculated torque.

5. CONCLUSIONS

The paper has proposed an electric machine for electrical power steering (EPS) system. Having in mind the advantages of a permanent magnet synchronous machine (PMSM), meaning its high power density and efficiency, with acceptable torque ripples, and knowing that one of the main demands of the application is to assure the fault tolerance capability, the authors have proposed a PMSM with 6 phases. Due to the specific winding displacement, it is sufficient to assure the control signals only via 3/6 PWM generators. By using the finite element method the authors have proved the machine's capability to operate in faulty conditions. Finally, the experimental results have emphasized the validity of the proposed design and the fact that the PMSM6 is a serious candidate for EPS applications.

ACKNOWLEDGMENT

This work was financially supported by CNCISIS-UEFISCDI, project type PN-II-RU, code TE-250, project number 32/28.07.2010.

REFERENCES

1. Larminie, J. and J. Lowry, *Electric Vehicle Technology Explained*, John Wiley & Sons, 2003.
2. Iles-Klumpner, D., "Automotive permanent brushless actuation technologies," PhD. Thesis, University Politehnica, Timisoara, Romania, 2005.

3. Ravaud, R., G. Lemarquand, V. Lemarquand, and C. Depollier, "The three exact components of the magnetic field created by a radially magnetized tile permanent magnet," *Progress In Electromagnetics Research*, Vol. 88, 307–319, 2008.
4. Zhao, W., M. Cheng, R. Cao, and J. Ji, "Experimental comparison of remedial single-channel operations for redundant flux-switching permanent-magnet motor drive," *Progress In Electromagnetics Research*, Vol. 123, 189–204, 2012.
5. Fuhs, A. E., *Hybrid Vehicles and the Future of Personal Transportation*, CRC Press, 2008.
6. *Bosch Automotive Handbook*, Robert Bosch GmbH, 2002.
7. Torkaman, H. and E. Afjei, "Hybrid method of obtaining degrees of freedom for radial airgap length in SRM under normal and faulty conditions based on magnetostatic model," *Progress In Electromagnetics Research*, Vol. 100, 37–54, 2010.
8. Gieras, J. F. and M. Wing, *Permanent Magnet Motor Technology*, Marcel Dekker Inc., New York, 2002.
9. Tessarolo, A., "On the modeling of poly-phase electric machines through vector-space decomposition: Theoretical considerations," *International Conference on Power Engineering, Energy and Electrical Drives*, 519–523, 2009.
10. Torkaman, H. and E. Afjei, "FEM analysis of angular misalignment fault in SRM magnetostatic characteristics," *Progress In Electromagnetics Research*, Vol. 104, 31–48, 2010.
11. Akrad, A., M. Hilairret, and D. Diallo, "Design of fault-tolerant controller based on observers for a PMSM drive," *IEEE Transactions on Industrial Electronics*, Vol. 58, 1416–1427, 2011.
12. Hanselman, D. C., *Brushless Permanent-magnet Motor Design*, McGraw-Hill, 1994.
13. Fodorean, D., A. Djerdir, I. A. Viorel, and A. A. Miraoui, "Double excited synchronous machine for direct drive application — Design and prototype tests," *IEEE Transactions on Energy Conversion*, Vol. 22, 656–665, 2007.
14. Akbari, H., H. Meshgin-Kelk, and J. Milimonfared, "Extension of winding function theory for radial and axial nonuniform air gap in salient pole synchronous machines," *Progress In Electromagnetics Research*, Vol. 114, 407–428, 2011.
15. Norhisam, M., S. Ridzuan, R. N. Firdaus, C. V. Aravind, H. Wakiwaka, and M. Nirei, "Comparative evaluation on power-speed density of portable permanent magnet generators for agricultural application," *Progress In Electromagnetics Research*,

- Vol. 129, 345–363, 2012.
16. Lecointe J.-P., B. Cassoret, and J.-F. Brudny, “Distinction of toothing and saturation effects on magnetic noise of induction motors,” *Progress In Electromagnetics Research*, Vol. 112, 125–137, 2011.
 17. Jian, L., G. Xu, Y. Gong, J. Song, J. Liang, and M. Chang, “Electromagnetic design and analysis of a novel magnetic-gear-integrated wind power generator using time stepping finite element method,” *Progress In Electromagnetics Research*, Vol. 113, 351–367, 2011.
 18. Mahmoudi, A., N. A. Rahim, and W. P. Hew, “Axial-flux permanent-magnet motor design for electric vehicle direct drive using sizing equation and finite element analysis,” *Progress In Electromagnetics Research*, Vol. 122, 467–496, 2012.
 19. Dib, N. I., S. K. Goudos, and H. Muhsen, “Application of Taguchi’s optimization method and self-adaptive differential evolution to the synthesis of linear antenna arrays,” *Progress In Electromagnetics Research*, Vol. 102, 159–180, 2010.
 20. Carro, P. L., C. J. De Mingo Sanz, and P. G. Ducar, “Radiation pattern synthesis for maximum mean effective gain with spherical wave expansions and particle swarm techniques,” *Progress In Electromagnetics Research*, Vol. 103, 355–370, 2010.
 21. Taboada, J. M., M. G. Araujo, J. M. Bertolo, L. Landesa, F. Obelleiro, and J. L. Rodriguez, “MLFMA-FFT parallel algorithm for the solution of large-scale problems in electromagnetics,” *Progress In Electromagnetics Research*, Vol. 105, 15–30, 2010.
 22. Touati, S., R. Ibtouen, O. Touhami, and A. Djerdir, “Experimental investigation and optimization of permanent magnet motor based on coupling boundary element method with permeances network,” *Progress In Electromagnetics Research*, Vol. 111, 71–90, 2011.